0013-4651/2008/155 9 /A615/8/$23.00 © The Electrochemical Society

Electrochemical Properties of Nanostructured $Al_{1-x}Cu_x$ Alloys as Anode Materials for Rechargeable Lithium-Ion Batteries

C. Y. Wang,[a,*] Y. S. Meng,[b,*] G. Ceder,[c,*,z] and Y. Li[a,d,z]

[a]Advanced Materials for Micro- and Nano-Systems Programme, Singapore-MIT Alliance, Singapore 117576
[b]Department of Materials Science and Engineering, University of Florida, Gainesville, Florida 32611, USA
[c]Department of Materials Science and Engineering, Massachusetts Institute of Technology, Cambridge, Massachusetts 02139, USA
[d]Department of Material Science and Engineering, National University of Singapore, Singapore 117574

The key challenge to use metallic alloys as anodes in rechargeable lithium batteries is to improve their cycling ability without compromising their high speciÞc capacity. We suggest that an important parameter controlling these two properties is the magnitude of interaction between the active and the inactive components in the alloy system. We demonstrated these ideas on the AlÐCu system by investigating the structure and electrochemical properties of sputtered $Al_{1-x}Cu_x$ $0 \le x \le 0.37$ thin-Þlm alloys. The optimum composition is determined to be 20 at % Cu. A speciÞc capacity of 792 mAh/g has been obtained for nanostructured $Al_{0.8}Cu_{0.2}$ with capacity retention of 50% after 100 cycles. The formation of a supersaturated solid solution structure is also suggested to enhance the electrochemical performance.
DOI: 10.1149/1.2943215

Manuscript submitted March 7, 2008; revised manuscript received May 12, 2008. Published July 2, 2008; publisher error corrected August 6, 2008.

Metallic anode materials for rechargeable lithium-ion batteries have been widely investigated because of the signiÞcant higher theoretical capacities compared to conventional graphite anodes.[1-4] For example, the theoretical capacities of metals, such as Si, Sn, and Al, are 3600, 990, and 993 mAh/g, respectively, compared to graphite with a capacity of 372 mAh/g.[2,3] However, the volume expansion of the lithiated alloys is also much larger than that of the lithiated graphite, leading to pulverization of the electrode and poor capacity retention.[4] The volume expansion of lithiated Si, $Li_{22}Si_5$, Sn, $Li_{22}Sn_5$, and Al, AlLi are 322, 260, and 96% as compared to graphiteÕs 9% volume expansion.[2,3] Thus, recent research work mostly focused on trying to minimize capacity loss by creating dimensionally stable alloys.

Many methods have been explored to improve the cycling ability of the metallic anodes. The mixed-conductor matrix concept, proposed by Boukamp et al. in the 1980s,[5] had a signiÞcant impact on metallic anode research. Using this concept, composites,[6-9] intermetallics,[10-16] and amorphous alloys[17-22] have been designed with particles of the reactive metal Þnely dispersed within a solid, mixed-conducting, metallic matrix. The inactive matrix reduces the relative volume expansion of the electrode and serves as a buffering component to reduce the materials displacement in the electrode induced by the volume expansion of the active materials. The key challenge to apply this concept is to strike a balance between cycling performance and electrochemical capacity in these mixed-conductor matrix materials. As an example, active component aggregation has been observed in Sn-based composites[6,7] and Sn_2Fe,[10] leading to capacity degradation. Courtney et al. reported that the Þnal cluster size of aggregated Sn particles was inversely proportional to the amount of inactive ions.[7] The cycling performance can generally be improved in these materials by increasing the amount of the inactive component at the expense of the electrochemical capacity. For some composite materials, such as Sn-based composite oxides,[6,7] SnÐFeÐC,[8] and SnÐMnÐC,[9] acceptable cycling ability could only be achieved with a large amount of inactive component, 60 to 87 at %, resulting in low speciÞc capacities around 150Ð300 mAh/g. Although many Si and Sn-based alloys have been evaluated,[10-16] the SnÐCoÐC system seems to have shown the best possibility of improving the cycling ability while retaining acceptable electrochemical capacity.[18,19] In 2005, Sony announced a commercialized product, Nexelion, using amorphous SnÐCoÐC alloy as an anode.[18] A speciÞc capacity of 670 mAh/g was reported for $Sn_{0.55}Co_{0.45}C_{0.4}$ without any capacity loss for up to 25 cycles.[19]

In this paper, we focus on binary Al-based alloys, because less progress has been made in these alloys compared to Si- and Sn-based materials. We will demonstrate how to select preferred inactive alloying elements based on the magnitude of their interaction with Al. $Al_{1-x}Cu_x$ $x = 0$, 0.01, 0.05, 0.1, 0.145, 0.2, 0.26, and 0.37 thin-Þlm alloys were prepared using cosputtering methods. The structure of the sputtered $Al_{1-x}Cu_x$ thin Þlms, their speciÞc capacity, and cycling ability as a function of Cu concentration were investigated.

Selection of Al-Based Alloy System for Anode Application

As discussed in the previous section, the cycling ability of an alloy system increases as the content of inactive component increases, while the speciÞc capacity decreases. We believe that the strength of the interaction between the active and the inactive component is a critical factor that determines how speciÞc capacity and cycling ability respond to the addition of the inactive component. If the inactive component has a strong attractive interaction with the Li-active component, then it signiÞcantly reduces the thermodynamic activity of the Li-active component, lowering the electrode voltage. Adding strongly interacting inactive elements therefore shifts the equilibrium potential down and may reduce the amount of Li that can be inserted. However, strong interaction may be beneÞcial to prevent aggregation because the strong bonding with the active material Al in our case may prevent Al from coarsening. This competing effect is an issue in particular for Al, which in its pure state already has a lower voltage against Li than materials such as Si or Sn. Hence, one cannot afford to lower the voltage too much with alloying element in binary Al alloys. Elements that weakly interact with Al do not severely reduce the activity of the active component to Li, but may be inefÞcient against aggregation of the active component. Hence, an inactive component with some intermediate strength of interaction with the active component may be preferred.

In order to prove our speculation, we studied the interaction between Al and several inactive alloying elements and its relationship to the electrochemical performance of the respective binary Al alloys. The relevant interaction is actually what is called the effective cluster interaction, as deÞned in Þrst-principles alloy theory[23] and is approximately equal to the difference between the A-B interaction and the average of the A-A and B-B interactions. This effective

* Electrochemical Society Active Member.
z E-mail: gceder@mit.edu; mseliy@nus.edu.sg

Figure 1. Formation enthalpies calculated using Þrst principles methods for Al-based intermetallic compounds.[24]

interaction is directly proportional to the enthalpy of mixing in the solid solution. The effective interactions between the constituent elements are estimated from the formation energies of the respective Al-based intermetallic compounds shown in Fig. 1. Data in Fig. 1 come from a Þrst-principles database.[24] The alloying elements can be divided into two groups based on the slope of their formation energies for low concentration of an alloying element. The Þrst group of compounds AlÐFe, AlÐNi, and AlÐMn has a higher slope in the formation energy than the second group of compounds AlÐMg and AlÐSb. This indicates a stronger interaction between Al and Fe or Ni, Mn than that between Al and Mg or Sb in the dilute alloying regime. Note that AlÐCu is intermediate between these two groups.

The electrochemical performance for some of these Al-based alloys has been previously reported,[25,29] and a correlation between the magnitude of the interaction and the electrochemical performance was found: For the Þrst group of alloys, such as AlÐFe, AlÐNi, and AlÐMn alloys, which have a strong interaction between the active and inactive elements, the speciÞc capacity has been reported to drop rapidly when the alloy composition increases beyond 4Ð6 at % and reaches zero when the composition of inactive component approaches 10Ð15 at %.[25,27] Al_6Mn (Mn = 14.3 at %) was also reported to have little capacity.[26] For the second group of alloys, such as AlÐMg and AlÐSb, only limited improvement in the cycling performance over pure Al was reported. For AlÐMg with 15 at % Mg, less pronounced fracture as compared to pure Al was observed after three cycles.[27] For AlÐSb, it was reported that the electrochemical cycling appeared to be limited by the difÞculty of reincorporating the extruded Al back into the Sb during the reverse reaction.[28,29]

AlÐCr shows similar electrochemical performance as the AlÐFe, AlÐMn, and AlÐNi systems.[25] The calculated formation energies of AlÐCr intermetallic compounds in Ref. 24 do not agree with those obtained from the experimental phase diagram through the Calphad method.[30] The AlÐCr system is therefore not included in our analysis.

Although the magnitude of interaction between Al and the alloying elements is a useful indicator of the enthalpy of mixing and, hence, activity reduction of the active component, the atomic arrangement (e.g., structure of an intermetallic) further affects the actual reaction enthalpy and, hence, the electrochemical performance.

Based on the above analysis, we select Cu as an alloying element because it has an intermediate effective interaction with Al, and little is known about the activity of AlÐCu alloys with Li.

Experimental Methods

Thin-Þlm deposition technique.ÑThe $Al_{1-x}Cu_x$ thin Þlms were produced using the sputtering tool Discovery 18 from Denton Vacuum, Inc. Al and Cu targets (3 in.) with purity of 99.99% from the Kurt. J. Lesker Company were used. The sputtering process was carried out under a base pressure of 5×10^{-6} Torr and Ar pressure of 2.25×10^{-2} Torr. A 12 mm diam circular-shaped Cu substrate was placed along the radial direction between the Al and Cu targets. The substrate stage does not rotate during the deposition to enable a composition gradient along the radial direction. Radio frequency power applied to the targets was tuned to adjust the sputtering rate. The $Al_{1-x}Cu_x$ thin Þlms under investigation were deposited using 200 W power for the Al target, and 40 or 55 W power for the Cu target.

Film characterization.ÑAfter deposition, the Þlm composition was analyzed with the energy dispersive X-ray technique (EDX) on a Philips XL-FEG scanning electron microscope (SEM). Calibration of the EDX results was carried out using Rutherford backscattering. Microstructures of the samples were analyzed using a Bruker X-Ray General Area Detector Diffraction System with a Cu K X-ray radiation, Philips XL-FEG SEM, and a Philip CM200 FEG transmission electron microscope (TEM) operating at 100 keV. Cross-sectional TEM samples were prepared using a FEI Nova 200 Dualbeam Focused Ion Beam. Top view TEM samples were prepared with a Precision ion polishing system 691. Film thickness was measured with a KLA Tencor, Alpha-step 500 surface proÞler. The weight of the samples was measured before and after Þlm deposition with a Þve-digit A&D HM-202 balance.

The Þlm thicknesses for all deposited samples are typically 200 nm. Eight different Cu compositions were used in this work: $Al_{1-x}Cu_x$ with x = 0, 0.01, 0.05, 0.1, 0.145, 0.2, 0.26, and 0.37. The compositions were measured at Þve different locations on the Þlm, and the Þnal value is taken as the average. The composition within the entire Þlm varies within a range of 5 at % as detected from Þlm-surface EDX on the SEM tool. The Þlm deposition rate is 20 nm/min, but there is a gradient 10% across the substrate because the stage was not rotating.

Electrochemical test.ÑLithium half-cells were assembled using a Swagelok battery set with 0.75 mm thick lithium foil as negative electrode and $Al_{1-x}Cu_x$ thin Þlms on a Cu substrate as positive electrode. Celgard 2500 microporous polyethylene membrane was used as the separator. The electrolyte was 1.0 M $LiPF_6$ in 1:1 ethylene carbonate–diethyl carbonate by volume ratio. Cells were assembled in an argon-Þlled glove box, where the moisture level was controlled at 0.1 ppm. All cells were tested using a Maccor MC-4 series battery tester. Constant current charge/discharge was carried out with voltage sweep from 0.01 to 1.2 V. Constant currents of 10, 50, and 100 A were used for different charge/discharge rates.

Results

Characterization of the sputtered $Al_{1-x}Cu_x$ thin Þlms.ÑAs the Cu content increases, different phases were observed by X-ray diffraction (XRD) and TEM as well as a general decrease in grain size. XRD spectra of the sputtered $Al_{1-x}Cu_x$ thin Þlms are shown in Fig. 2. In the as-sputtered Þlms, no additional peaks, other than Al peaks, were observed for samples with up to 20 at % Cu. This indicates Al–Cu solid-solution formation in this composition range. For the sample with 26 at % Cu, the presence of Al and Al_2Cu peaks indicates that two phases, Al and Al_2Cu, coexist. For the sample with 37 at % Cu, only the Al_2Cu peaks are present. The phases observed as functions of composition are summarized in Table I. It is also observed that the heights of the Al peaks decrease and the widths increase as the Cu content increases, an indication of the decrease in grain size. On the basis of the Scherrer equation,[31] the grain size of the sputtered $Al_{0.8}Cu_{0.2}$ solid solution is estimated to be 10 nm.

Because Cu is used as the substrate, it is difÞcult to judge whether the Cu phase exists in the Þlm from the XRD results. TEM and selected area diffraction (Fig. 3) of the sample with 20 at % Cu was therefore carried out for further structure and phase analysis. High-resolution TEM shows a nanocrystalline columnar structure with grains around 5Ð10 nm. Between the grains are large portions

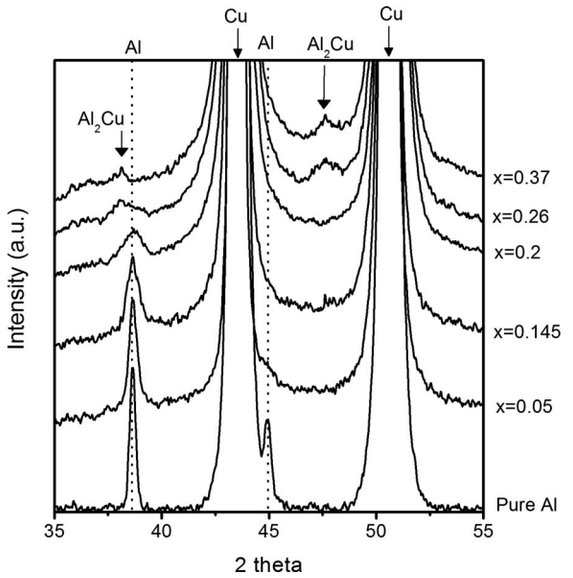

Figure 2. XRD spectra of the as deposited $Al_{1-x}Cu_x$ x = 0, 0.05, 0.145, 0.2, 0.26, and 0.37 thin films. Al peaks are highlighted by the dashed lines. Al_2Cu peaks are indicated by arrows. Cu peaks are from the Cu substrate.

of noncrystalline interfacial structure. Selected area diffraction shows that the phase present has a face-centered-cubic structure with the d-spacing slightly larger than that for pure Al,[32] indicating the formation of supersaturated solid solution for $Al_{0.8}Cu_{0.2}$. Cu phase was not detected. The possibility of the existence of Cu phase in $Al_{0.8}Cu_{0.2}$ film is therefore excluded. EDX results from the film cross-sectional TEM sample show the Cu content in the film varies within a range of 7%.

Table I. Summary of the phase formation for sputtered $Al_{1-x}Cu_x$ thin-film alloys.

Cu at % composition	0	5	14.5	20	26	37
Phase	Al	AlCu	Al Cu	Al Cu	Al Cu /Al_2Cu	Al_2Cu

Galvanostatic charge–discharge test.—Specific capacity and cycling ability of the $Al_{1-x}Cu_x$ thin-film alloys.—Charge–discharge cycles were conducted between 0.01 and 1.2 V at 100, 50, and 10 A constant current, and typical charge–discharge curves of pure Al, $Al_{0.855}Cu_{0.145}$, $Al_{0.8}Cu_{0.2}$, and $Al_{0.74}Cu_{0.26}$ at 10 A are shown in Fig. 4a-d. In Fig. 4e, we summarize the change of specific capacity as a function of cycle number. For pure Al, the capacity decreases rapidly with increasing cycles, and reaches almost zero after 20 cycles. For $Al_{0.855}Cu_{0.145}$, the capacity fading is slower compared to that of pure Al, but the capacity becomes very small after 40 cycles. For $Al_{0.8}Cu_{0.2}$, the capacity fading is much slower and the capacity retention is 388 mAh/g, 50% of its initial capacity, even after 100 cycles. For $Al_{0.74}Cu_{0.26}$, the capacity retention is 25% after 100 cycles. The capacity retention is higher with increasing Cu content, but the specific capacity is reduced as shown in Fig. 4a-d. The value of the first discharge capacity of pure Al, $Al_{0.855}Cu_{0.145}$, $Al_{0.8}Cu_{0.2}$, and $Al_{0.74}Cu_{0.26}$ are 1174, 940, 792, and 407 mAh/g, respectively. An optimum composition seems to be 20 at % Cu. The cycling ability of $Al_{0.8}Cu_{0.2}$ is significantly improved over pure Al, and the initial specific capacity remains high.

Cu composition effect on average potential.—To compare the potentials of the different Al–Cu alloys, we define the average potentials as the average of the charge and discharge potentials. For example, for pure Al we observe the discharge plateau at 0.192 V and the charge plateau at 0.494 V, giving an average of 0.343 V. This corresponds to the potential of the two-phase reaction of the Al Li solid solution to the AlLi phase.[33,34] As the Cu composi-

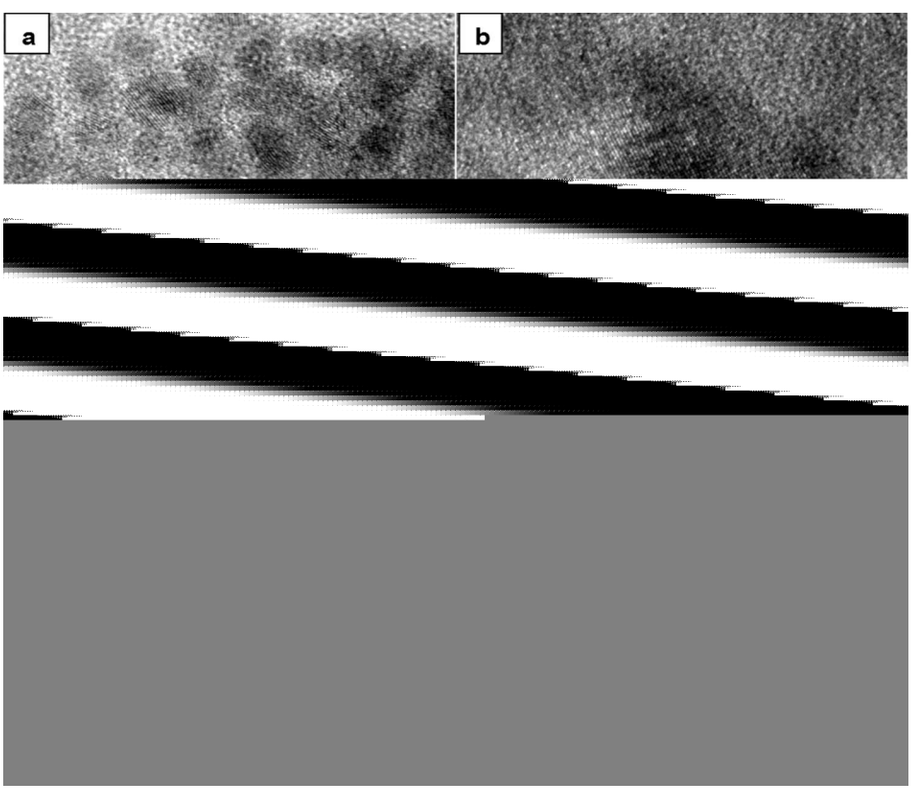

Figure 3. a Top view TEM, b, c cross-sectional TEM, and d diffraction, for the as deposited $Al_{0.8}Cu_{0.2}$ film. c: Cu to Al ratio detected by EDX at different sites: 1 = 29:71, 2 = 27:73, 3 = 33:67, 4 = 30:70, and 5 = 26:74. D-spacing for pure Al,[32] 111: 2.338A, 200: 2.024A, 220: 1.431A, 311: 1.221A.

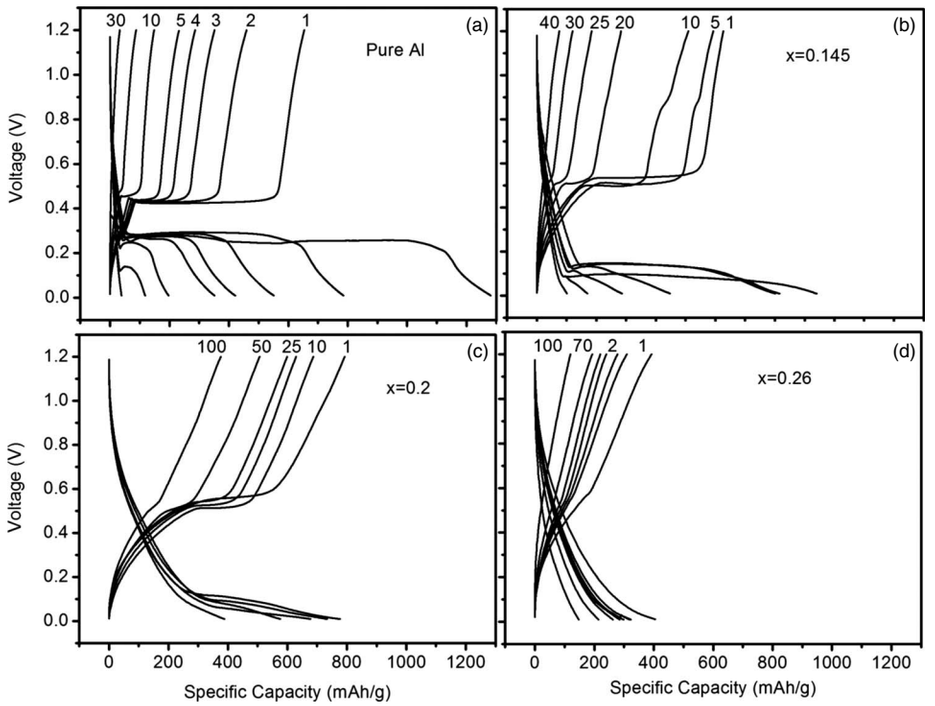

Figure 4. Charge/discharge curves for the battery with a pure Al anode, b $Al_{0.855}Cu_{0.145}$, c $Al_{0.8}Cu_{0.2}$, and d $Al_{0.74}Cu_{0.26}$ at current of 10 uA. e Specific capacity as a function of cycle number for a–d.

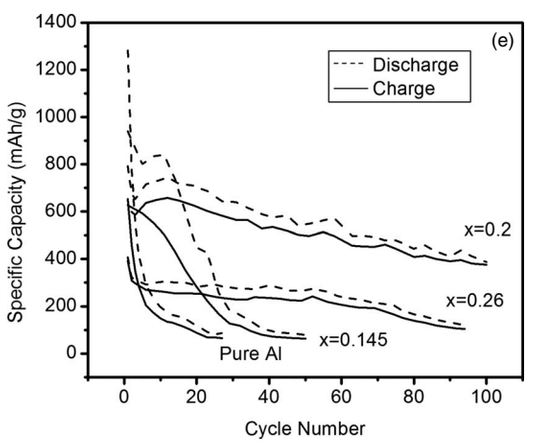

tion increases, a decrease in the first-cycle average potential is observed Fig. 5. To confirm our observation, we measured the average potential on two or three samples for each composition and consistently observed a decrease in average potential with an increase in Cu composition in the film. A similar observation was reported in the Sn–Co system,[19] where the average potential of the first cycle decreased with increasing Co in the alloy. In our work, we attribute this decrease in potential to the Al activity reduction as more Cu is added to the alloy. It shall be noted that because the average potential is not the equilibrium potential, variations in diffusion or other kinetic factors may also contribute to a change in average potential with Cu content.

Grain-size effect on the shape of the charge/discharge curves and the nucleation potential. We observe in Fig. 4a that the charge/discharge curves of pure Al are mainly composed of plateau regions, while those of $Al_{0.855}Cu_{0.145}$ and $Al_{0.8}Cu_{0.2}$ Fig. 4b and c consist of a sloped and a plateau region. As the Cu content increases, the sloped portion on the charge/discharge curves also increases. For $Al_{0.8}Cu_{0.2}$ Fig. 4c, it contributes 50% of the capacity. We believe that the capacity in the sloped region may be due to the random interfacial or intergranular component, which increases as the grain

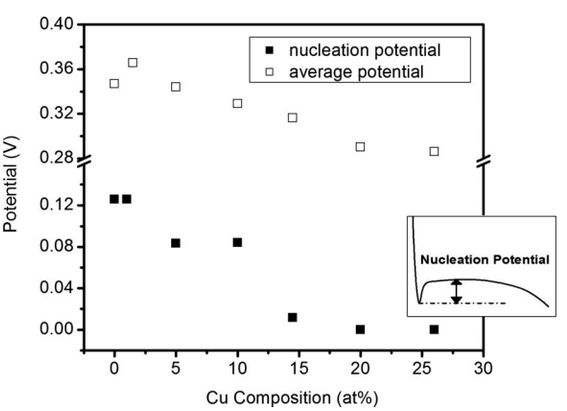

Figure 5. First discharge nucleation potential and first cycle average potential of the lithiation reaction as a function of Cu composition.

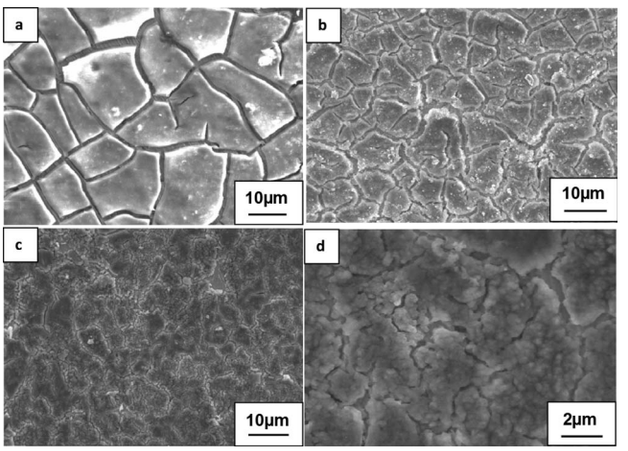

Figure 6. SEM of a pure Al cycling after 20 cycles, b $Al_{0.9}Cu_{0.1}$ after 20 cycles, and c, d $Al_{0.8}Cu_{0.2}$ after 100 cycles.

size decreases. From TEM Fig. 3a, it is observed that the grain size is around 5–10 nm with a large portion of the noncrystalline interfacial component in the $Al_{0.8}Cu_{0.2}$ sample. Gleiter[35] proposed that when the grain size is around a few 1–10 nanometers, these materials consist of two components, a crystalline component and an interfacial component, whose volume fraction is 50% each. According to the results from XRD, Mossbauer spectroscopy, and extended X-ray absorption fine structure, the grain boundary structure in the nanomaterials was proposed as "gaslike," a kind of "random structure" with the absence of long- and short-range order.[36-38] We therefore attribute the capacity of the sloped region to the noncrystalline interfacial component and the capacity in the plateau to the crystalline component.

We also define the discharge nucleation potential as the small dip in the discharge curve, corresponding to the extra energy required to nucleate the AlLi phase in AlCu solid solution as shown in Fig. 5. It is well known that some overpotential is required to nucleate lithiated compounds in metallic alloys.[39] Figure 5 shows that the nucleation potential on first discharge decreases as the Cu content increases. We attribute this trend to the decrease in the grain size of the Al Cu solid solution, and the increased disordered fraction as the Cu content increases. If the crystal size is below the size of a critical nucleus, then the energy required to overcome the nucleation barrier will decrease with grain size. The presence of more disordered material in higher Cu content alloys may also be a factor, allowing for easier heterogeneous nucleation. The nucleation potential is reduced to around zero for $Al_{0.8}Cu_{0.2}$ with grain size around 5–10 nm.

Characterization of the $Al_{1-x}Cu_x$ thin films after cycling.— The batteries were disassembled after cycling and studied with SEM to investigate structure changes in the samples. SEM images of pure Al after 20 cycles, $Al_{0.9}Cu_{0.1}$ after 20 cycles and $Al_{0.8}Cu_{0.2}$ after 100 cycles are shown in Fig. 6. Deep and wide cracks can be observed on the samples of pure Al and $Al_{0.9}Cu_{0.1}$. A large portion of the electrode is peeled off from the substrate for these two samples. Much milder cracks are observed for the $Al_{0.8}Cu_{0.2}$ sample, even after 100 cycles, and the electrode as a whole did not peel off and remained intact.

TEM was also conducted to further study, in more detail, the structural changes in the $Al_{0.8}Cu_{0.2}$ thin film. Figures 7a and b show bright- and dark-field cross-sectional TEM images for the charged $Al_{0.8}Cu_{0.2}$ sample after 100 cycles. The columnar structure is broken, and instead, grains of about 10–20 nm are observed Fig. 7b. Compared to the sample before cycling Fig. 3c, we observe more variation in image contrast, probably caused by volume expansion

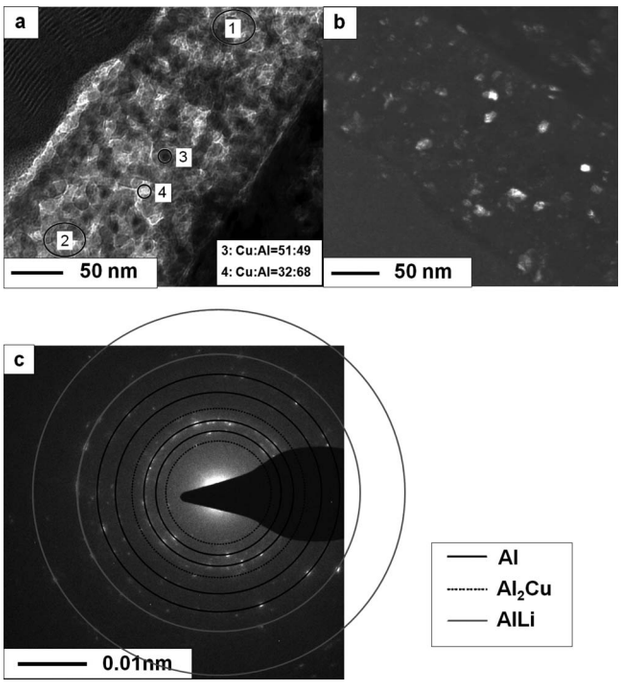

Figure 7. Cross sectional a bright field, b dark-field TEM, c diffraction for $Al_{0.8}Cu_{0.2}$ after 100 cycles. a: Cu to Al ratio detected by EDX: 1 = 42:58, 2 = 37:63, 3 = 51:49, and 4 = 32:68.

induced fractures. Observations in Fig. 7a and b confirmed that the $Al_{0.8}Cu_{0.2}$ film was still attached to the substrate even after 100 cycles without peeling off.

The diffraction pattern Fig. 7c, indicates that Al and AlLi are the dominant crystalline phases. Some weak diffraction of Al_2Cu is also observed. The reason for the formation of Al_2Cu will be discussed later. The EDX results show that after cycling the Cu content in the $Al_{0.8}Cu_{0.2}$ film becomes less uniform—range 19% than before cycling range 7% Fig. 4c. This may be caused by the formation of Al_2Cu with a higher Cu concentration. Nevertheless, we did not detect clusters of Al atoms. The Cu content at all the sites sampled after cycling—as small as 10–20 nm regions—is still high. This indicates that aggregation of Al atoms did not occur.

Discussion

Specific capacity of $Al_{1-x}Cu_x$ as a function of Cu composition.— The first discharge capacities of the sputtered $Al_{1-x}Cu_x$ thin films at 10 uA current are shown in Fig. 8. The experimental data points for the box plot are taken as the average capacity from two to three samples. The solid line is a model for the specific capacity explained below.

Similar to the model in Ref. 25, we describe the experimental specific capacity by three regions in which the specific capacity decreases differently with Cu content. Region I corresponds to a composition range from 0 to 20 at %, in which AlCu solid solution forms, as observed in the XRD. The measured capacities in this region are equal to those expected from a combination of active Al and inactive Cu. The specific capacity can therefore be explained by a simple displacement reaction

$$Al_{1-x}Cu_x + Li \quad 1 - x\ AlLi + xCu \qquad (1)$$

It is possible that the AlLi phase dissolves some Cu so that less Cu transport is needed, but we cannot determine this from the data available. As the Cu content increases beyond 20 at %—region II, the specific capacity drops more rapidly. The capacity in region II can be explained by a coexistence of AlCu and Al_2Cu. The for-

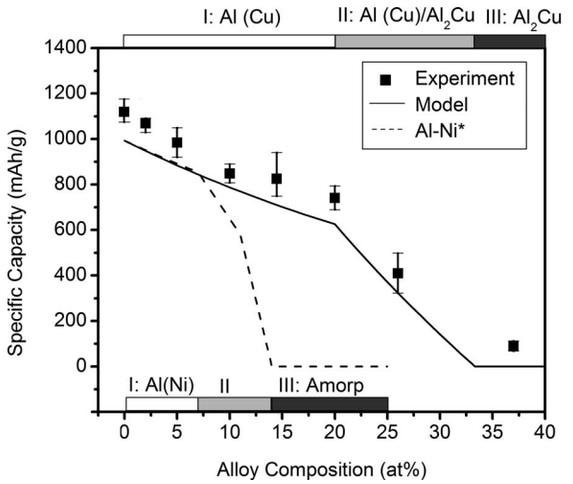

Figure 8. First cycle specific-capacity discharge change as a function of Cu composition. Box plot data points are from the experimental electrochemical test under 10A constant current. Solid line is the specific capacity of Al–Cu predicted by the model described in the text; dotted line is the specific capacity of Al–Ni predicted by a model from previous work.[25] The three regions labeled with different phases are discussed in the main text.

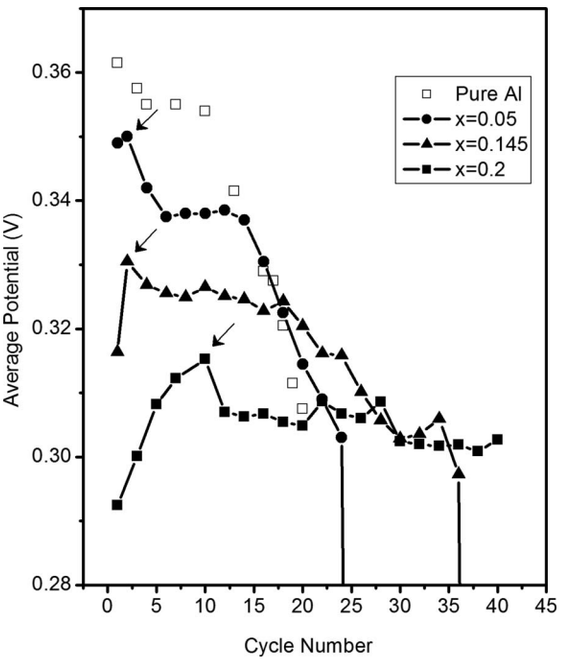

Figure 9. Evolution of the average potential evolution with cycles for pure Al and $Al_{1-x}Cu_x$ $x = 0.05$, 0.145, and 0.2 alloys.

mation of Al, Cu, and Al_2Cu in this composition range from 20 to 33.3 at % is consistent with the XRD resutls in Fig. 2. It is reported that Al_2Cu has little capacity as an anode material in lithium-ion battery.[26] In this region, only the Al atoms in the Al_2Cu phase react with Li according to the reaction in Eq. 1. The capacity in region II drops rapidly as every Cu atom added removes two Al atoms from the electrochemical active subsystem. When the composition reaches 33.3 at % Cu, only Al_2Cu is present and the specific capacity is zero (region III).

In region II, $Al_{1-x}Cu_x$ is assumed to be made up of a mole fraction of $2.5–7.5x$ $Al_{0.8}Cu_{0.2}$ and $2.5x–0.5$ of Al_2Cu. The capacity can be calculated as follows

$$\text{capacity} = \frac{2\,(1 - 3x)\,F}{(1 - x)\,W_{Al} + xW_{Cu}} \qquad (2)$$

F is the Faraday's constant, W_{Al} is the molecular weight of Al, W_{Cu} is the molecular weight of Cu, x is the composition of Cu. Only the Al atoms in active $Al_{0.8}Cu_{0.2}$ are included in the capacity calculation.

The specific capacity expected from the above model has been plotted as a solid line and compared to our experimental results in Fig. 8. Reasonably good agreement between the model and the experimental results is observed, except that the measured capacities are general higher by an amount of 50–150 mAh/g even for pure Al. The additional capacity is attributed to the native Cu oxide. When a bare Cu substrate was cycled as an anode, a similar amount of capacity was obtained. It is known that Cu oxide reacts with Li.[40] Inaccuracy in the measurement of film mass could be another reason, causing the large spread in the capacity, though it is unlikely that this would show up as a systematic shift in capacity in the data.

In order to compare to our results in the Al–Cu system, the specific capacity model of sputtered Al–Ni thin-film alloys from previous work[25] is also included in Fig. 8. In Al–Ni, the specific capacity was also reported to decrease at different rates in three regions. Region I corresponds to Al–Ni solid solution, where all Al are active to Li; region II is described by a coexistence between Al–Ni solid solution and an inactive amorphous Al–Ni phase; region III corresponds to amorphous Al–Ni and compounds with more Ni. For both Al–Cu and Al–Ni, the specific capacity decreases as the amount of inactive element increases, but the rate of decrease with alloying concentration is much slower for Al–Cu. Because the interaction between Al and Cu is weaker than that between Al and Ni, Cu does not reduce the activity of Al as much as Ni does. As a result, only when the Cu content reaches 33.3 at %, the sample is single-phase inactive Al_2Cu and the specific capacity drops to zero. In Al–Ni–Fe, Mn alloys, however, an inactive phase already forms at 10 to 15 at %. As the formation enthalpy of Al_2Cu is less than the formation enthalpy of the compounds in Al–Ni, Al–Fe, and Al–Mn, the Al phase also allows for more Cu solubility. Because solid solution is the most effective way of retaining capacity on alloying and Al remains active, this mechanism also increases the specific capacity in the Al–Cu system. Up to 25 at % Cu can be added in the Al–Cu system while retaining a specific capacity higher than that of graphite (372 mAh/g). Because of the wide range of Cu compositions with reasonable capacity, it is easier to locate an optimum composition for the Al–Cu system than for the Al–Ni system.

Structural and compositional change of $Al_{1-x}Cu_x$ thin-film alloys over cycling.—A significant improvement in cycling ability was observed for the sample with 20 at % as observed in Fig. 4e. To understand in detail how Cu plays a role in the cycling ability of Al–Cu alloys, we studied the structural and compositional change of the $Al_{1-x}Cu_x$ thin films with electrochemical cycling. Many techniques have been employed in previous work to study the structural changes upon cycling of metallic alloys, such as in situ x-ray XRD,[41,42] and atomic force microscopy.[43,44] In our work, instead we track the average potential and nucleation potential to monitor the compositional and structural change with cycles.

The average potential of $Al_{1-x}Cu_x$ decreases as x increases in Fig. 5. This gives an indication that the change in average potential can be used to monitor the change in Cu composition in the active Al–Cu solid solution as the material is cycled. Figure 9 shows the average potential as a function of cycle number for pure Al, $Al_{0.95}Cu_{0.05}$, $Al_{0.855}Cu_{0.145}$, and $Al_{0.8}Cu_{0.2}$. For pure Al, it is observed that the average potential decreases over cycles accompanied by capacity fading. This effect can be explained by the fact that when the capacity decreases, the amount of active Al is reduced and, consequently, the increase in the effective charging rate relative to the amount of active material leads to a decrease in average potential. For $Al_{1-x}Cu_x$ $x = 0.05, 0.145, 0.2$ alloys, three stages are ob-

served in the evolution of the average potential. In the first stage, the average potential increases, indicating a decrease in the Cu composition in active Al–Cu solid solution on cycling. In the second stage, the average potential stabilizes for five to seven cycles, during which there is no more reduction in Cu composition. This indicates the beginning of the reversible cycling of the Al rich Al–Cu solid solution. In the third stage, capacity loss starts to occur and the average potential decreases because the relative charging rate increases as capacity is lost. We consistently observed this evolution of the average potential in three stages for two or three samples at each composition. A similar observation is reported in Sn–Co alloys in Ref. 19.

The average potential decreases at a much slower rate for the sample with 20 at % Cu as compared to other samples, indicating a much better cycling ability for this sample. It should also be pointed out that for Al–Cu solid-solution samples, the maximum average potential at the end of stage I, indicated by an arrow in Fig. 9, is lower than that of pure Al, indicating that, although the Cu composition in the Al–Cu solid solution has decreased, pure Al phase extrusion does not occur.

On the basis of the discussion in the section on grain-size effect on the charge/discharge curves and the nucleation potential, the change in nucleation potential can be used to monitor the change in the grain size in the active Al–Cu solid solution as the material is cycled. For pure Al, we observed that the nucleation potential decreases over cycles accompanied by capacity fading, suggesting the occurrence of pulverization—data are not shown in this paper. For $Al_{0.8}Cu_{0.2}$, we can observe in Fig. 4c, that there is no dip in the discharge curve for $Al_{0.8}Cu_{0.2}$ even after 100 cycles, indicating that the nucleation potential remains zero. This means that grain growth does not occur for this sample over cycling.

We suggest that the decrease in Cu composition in stage I is related to the Li extraction reaction. As proposed in Eq. 1, the first cycle Li insertion reaction is $Al_{1-x}Cu_x + Li \rightarrow AlLi + Cu$. Upon charging, Li is extracted from the electrode and the recombination process of the remaining Al and Cu determines the Cu composition in the active Al–Cu solid solution. On the basis of the presence of Al_2Cu in the EDX and diffraction (Fig. 6), we suggest that the following reaction occurs during the first cycle charging

$$(3 - y)\,AlLi + (1 + y)\,Cu \rightarrow (3 - y)\,Li + Al_{1-y}Cu_y + Al_2Cu \qquad (3)$$

It is reasonable to have Al_2Cu phase precipitation because the sputtered Al–Cu solid solutions are metastable at Cu composition higher than the thermodynamic solid solubility limit, 0.04 at % at room temperature,[45] and as such, there is no reason for them to reform upon charging. Using the relation between the average potential and Cu composition in Fig. 5, we can estimate the remaining Cu composition in the active Al–Cu solid solution at the end of stage I. For $Al_{0.95}Cu_{0.05}$, the Cu composition drops from 5 to 4.6 at %, $Al_{0.855}Cu_{0.145}$ from 14.5 to 9.8 at %, and $Al_{0.8}Cu_{0.2}$ from 20 to 13.8 at %, respectively. In stage II, a steady state is reached and no further Al_2Cu formation occurs. For $Al_{1-x}Cu_x$ alloys with higher Cu content, more Al_2Cu forms in stage I. However, because of the higher initial Cu composition for $Al_{0.8}Cu_{0.2}$, there is still a larger amount of Cu remaining in the active Al–Cu solid solution. This might be the reason why $Al_{0.8}Cu_{0.2}$ shows a much better cycling ability as compared to other $Al_{1-x}Cu_x$ alloys. Approximately 13.8 at % Cu remains in the $Al_{0.8}Cu_{0.2}$ thin film and serves as a buffering component for the volume expansion during Li insertion and as an agent to slow down Al extrusion and coarsening.

Our observations can be compared to other metallic alloy systems. A model for the aggregation of tin in tin oxide composite glasses was set up by Beaulieu and Dahn. They observed that Sn atoms from the initial well-dispersed state begin to aggregate into clusters of tens of atoms and that aggregation will proceed until the distance between tin clusters reaches some equilibrium length. In this case, the equilibrium tin cluster size depends on the initial volume fraction of tin in the glass. In this work, we proposed that the aggregation process depends not only on the volume fraction of the active component but also on the interaction between the active and inactive component. If the active and inactive components strongly interact, then less pure phase of the active component is formed, which reduces the driving force for aggregation. Our results indeed indicate that the presence of Cu reduces the amount of pure Al phase formed. In comparison, in SnF_2 anodes, Sn aggregation was observed after five cycles.[10] For Sn–Co, even with 47 at % Co, Sn aggregation was still observed.[19] Al aggregation is also believed to be the reason that limits the electrochemical cycling performance in Al–Sb.[28,29] For Al–Cu alloys, no Al aggregation is observed with only 20 at % Cu. We attribute the good performance of $Al_{0.8}Cu_{0.2}$ to the interaction between Cu and Al, which is neither too strong to reduce the Al activity nor too weak to cause aggregation during cycling. Because of the attractive interaction between Al and Cu, Al–Cu solid solutions reform during the charge process, though with reduced Cu composition. As a result, the Al aggregation process is restrained. A similar reformation reaction was reported in FeF_2.[10] However, the reformation of FeF_2 only continued for a few cycles and Sn aggregation ultimately occurred.

Effect of the formation of supersaturated Al (Cu) solid solution on thermodynamics of Al (Cu) solid solution.—To study how the formation of supersaturated Al–Cu solid solutions affects the electrochemical performance, we need to understand their thermodynamic properties. We determine the reaction enthalpy of the $Al_{1-x}Cu_x$ thin films from the average potential. Writing the lithiation reaction of the $Al_{1-x}Cu_x$ solid solution, normalized to half a Li reacted, gives

$$\frac{0.5}{1-x}Al_{1-x}Cu_x + 0.5Li \rightarrow Al_{0.5}Li_{0.5} + \frac{0.5x}{1-x}Cu \qquad (4)$$

The reaction enthalpy for this reaction is then 0.5 times the measured voltage[46]

$$H_{react} \approx G_{react} = -zFE \qquad (5)$$

E is the measured reaction potential, F is Faraday's constant, z = 0.5; G_{react} is the reaction Gibbs free energy. The average potentials of charge and discharge are taken as the reaction potentials. Whenever nonequilibrium reactions participate in the electrochemical process, error is introduced in this analysis. This is the case for the precipitation of Al_2Cu in the charge process, which is irreversible. However, this error in the average potentials can be neglected due to the small amount of Al_2Cu precipitation in each cycle. For $Al_{0.8}Cu_{0.2}$, the change in Cu composition per cycle in the reformed Al–Cu solid solution is 0.62 at % as determined from the potential.

The reaction enthalpies for Reaction 4 are plotted in Fig. 10. Data for the ground-state intermetallics from various sources are shown as well, for comparison. The calculated enthalpies are taken from first-principles calculations,[24] Calphad computation,[30] and thermochemical measurements.[47] These studies present formation enthalpies for Al–Cu compounds and for AlLi, from which we derive the reaction enthalpy as follows

$$H_{react} = H_{form}(Al_{0.5}Li_{0.5}) - \frac{0.5}{1-x}H_{form}(Al_{1-x}Cu_x) \qquad (6)$$

$H_{form}(Al_{0.5}Li_{0.5})$ are taken from first principles calculation, Calphad computation, and thermochemical database, respectively. The shift of the reaction enthalpy up or down in Fig. 10 is mainly caused by the difference in $H_{form}(Al_{0.5}Li_{0.5})$ in the different methods.

Effect of the formation of Al (Cu) supersaturated solid solution on the specific capacity and cycling ability.—The reaction enthalpy increases as the Cu composition increases for both Al solid solution experiments and Al–Cu intermetallics calculations, indicating the activity of Al to Li is reduced as the Cu composition increases. In return, this will give a lower potential against Li. There are several benefits to the fact that the Al–Cu solid solution is re-